DEPARTMENT OF MATHEMATICAL SCIENCES
COLLEGE OF SCIENCES
OLD DOMINION UNIVERSITY
NORFOLK, VIRGINIA 23529

THEORETICAL STUDIES OF LASERS AND CONVERTERS

By

John H. Heinbockel, Principal Investigator

Progress Report
For the period July 1, 1991 to December 31, 1991

Prepared for
National Aeronautics and Space Administration
Langley Research Center
Hampton, Virginia 23665

Under
Research Grant NAG-1-757
Dr. Robert C. Costen, Technical Monitor
SSD-High Energy Science Branch

(NASA-CR-189482) THEORETICAL STUDIES OF LASERS AND CONVERTERS Progress Report, 1 Jul. - 31 Dec. 1991 (Old Dominion Univ.) 33 p
CSCL 20E
N92-14333
Unclas
G3/36 0053159

November 1991

DEPARTMENT OF MATHEMATICAL SCIENCES
COLLEGE OF SCIENCES
OLD DOMINION UNIVERSITY
NORFOLK, VIRGINIA 23529

THEORETICAL STUDIES OF LASERS AND CONVERTERS

By

John H. Heinbockel, Principal Investigator

Progress Report
For the period July 1, 1991 to December 31, 1991

Prepared for
National Aeronautics and Space Administration
Langley Research Center
Hampton, Virginia 23665

Under
Research Grant NAG-1-757
Dr. Robert C. Costen, Technical Monitor
SSD-High Energy Science Branch

November 1991

PROGRESS REPORT NASA GRANT NAG1-757
ODURF 176615

THEORETICAL STUDIES OF LASERS AND CONVERTERS

We have previously examined Doppler broadening and its effects upon the stimulated emission cross-section σ_{ij} connecting an upper level (i) with a lower level (j) for an iodine laser. The stimulated emission cross-section is given by (reference 1),

$$\sigma_{ij} = \frac{\lambda^2 A_{ij}}{8\pi} g_{ij}(\nu) \tag{1}$$

where, $g_{ij}(\nu)$ is the normalized line shape function

$$g_{ij}(\nu) = \frac{2}{\pi\,\Delta\nu\left(1+4\left[\frac{\nu-\nu_{ij}}{\Delta\nu}\right]^2\right)}. \tag{2}$$

The level transitions for the iodine laser are illustrated in the figure 1. The relative intensities of these transitions are illustrated in figure 2.

The Einstein coefficients for the different lines have the transition rates

$$\begin{aligned} A_{34} &= 5.0\alpha & A_{23} &= 2.3\alpha \\ A_{33} &= 2.1\alpha & A_{22} &= 3.0\alpha \\ A_{32} &= 0.6\alpha & A_{21} &= 2.4\alpha \end{aligned} \tag{3}$$

in units of $\sec^{-1}$, where $\alpha = A/7.77$ with $A = 5.4 \pm 2.0\sec^{-1}$. Using

$$\nu_0 = \frac{c}{1.315246(10)^{-4}} = 2.28094(10)^{14} \approx 2.3(10)^4\,\text{GHz}, \tag{4}$$

the laser emission frequencies from ν_0 are given by

$$\begin{aligned} \nu_{34} &= \nu_0 & \nu_{21} &= \nu_0 - 0.427c \\ \nu_{33} &= \nu_0 + 0.141c & \nu_{22} &= \nu_{21} - 0.026c \\ \nu_{32} &= \nu_{33} + 0.068c & \nu_{23} &= \nu_{22} - 0.068c \end{aligned} \tag{5}$$

and consequently the overall stimulated emission cross-section is given by

$$\sigma = \frac{\lambda^2}{4\pi^2\Delta\nu}\left\{\frac{5}{12}\sum_{i=1}^{3}\frac{A_{2i}}{1+\left[2\left(\frac{\nu-\nu_{2i}}{\Delta\nu}\right)\right]^2} + \frac{7}{12}\sum_{i=2}^{4}\frac{A_{3i}}{1+\left[2\left(\frac{\nu-\nu_{3i}}{\Delta\nu}\right)\right]^2}\right\} \tag{6}$$

which is based upon statistical weights of the hyperfine levels (reference 1) and

$$\Delta\nu = \alpha_0 + \alpha_1 p \tag{7}$$

with $\alpha_0 = 2.51(10)^8\sqrt{T/300}$, $\alpha_1 = 1.88(10)^7\sqrt{T/300}$, where p is the pressure in torr, and T is the temperature in degrees Kelvin. Here α_0 is related to the Doppler line width and α_1 is the pressure broadening coefficient associated with the lasant $n - C_3F_7I$.

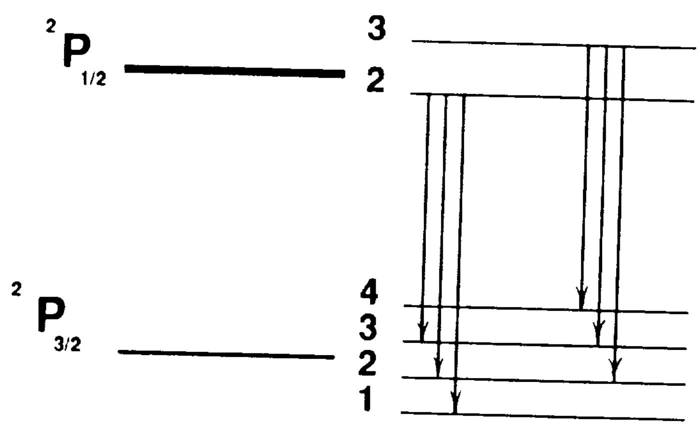

Figure 1. Level transitions for iodine.

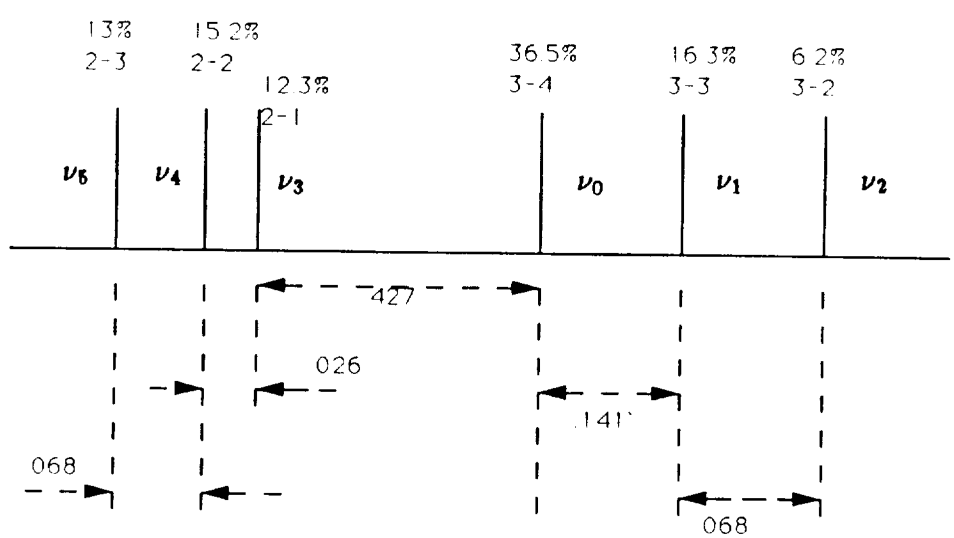

Figure 2. Relative intensities for iodine transitions

The Voigt Profile

The Voight profile considers the effect of both Doppler broadening and collision broading upon the absorption line shape. For homogeneous broadening it is assumed that every atom behaves in the same way. In this case the line shape function has a Lorentzian form. If a select group of atoms emit a frequency ν_{ij} in their rest frame and the rest frame moves with velocity v_z, then their exits a Doppler shift frequency and line shape function for the group. In particular, a group of atoms identified with a velocity component v_z has the shifted line shape function (references 2,3)

$$g(\nu, v_z) = \frac{2}{\pi\,\Delta\nu\left(1 + 4\left[\frac{\nu - \nu_{ij} + \nu_{ij}\frac{v_z}{c}}{\Delta\nu}\right]^2\right)} \tag{8}$$

where the fraction of atoms within the velocity range v_z and $v_z + dv_z$ is given by the Maxwell-Boltzmann distribution

$$\frac{dN}{N} = \left(\frac{M}{2\pi kT}\right)^{1/2} \exp\left(\frac{-Mv_z^2}{2kT}\right) dv_z \tag{9}$$

Multiplying equations (8) and (9) and integrating over all velocities, produces the Voigt profile line shape function

$$g_{ij}(\nu) = \left(\frac{M}{2\pi kT}\right)^{1/2} \int_{-\infty}^{\infty} \left\{ \frac{2}{\pi\,\Delta\nu\left(1 + 4\left[\frac{\nu - \nu_{ij} + \nu_{ij}\frac{v_z}{c}}{\Delta\nu}\right]^2\right)} \right\} \exp\left(\frac{-Mv_z^2}{2kT}\right) dv_z$$

or

$$g_{ij}(\nu) = \left(\frac{M}{2\pi kT}\right)^{1/2} \int_{-\infty}^{\infty} \frac{2\Delta\nu \exp\left(\frac{-Mv_z^2}{2kT}\right) dv_z}{\pi\left[(\Delta\nu)^2 + 4(\nu - \nu_{ij} + \nu_{ij}\frac{v_z}{c})^2\right]}. \tag{10}$$

The above integral is simplified by making the change of variables

$$y^2 = \frac{Mv_z^2}{2kT} \qquad dy = \left(\frac{M}{2kT}\right)^{1/2} dv_z \tag{11}$$

$$c_{ij} = 2\nu_{ij}\left(\frac{2kT\ln 2}{Mc^2}\right)^{1/2} \tag{12}$$

$$b_{ij} = (\ln 2)^{1/2}\frac{\Delta\nu}{c_{ij}} \tag{13}$$

$$x_{ij} = 2(\ln 2)^{1/2}\frac{\nu - \nu_{ij}}{c_{ij}}. \tag{14}$$

We can then express the line shape function in the form

$$g_{ij}(\nu) = \frac{2}{\pi^{1/2}\,\Delta\nu} \int_{-\infty}^{\infty} \frac{\ln 2 \left(\frac{\Delta\nu}{c_{ij}}\right)^2 e^{-y^2}\,dy}{\pi\left[\ln 2\left(\frac{\Delta\nu}{c_{ij}}\right)^2 + \left(\frac{2(\nu-\nu_{ij})(\ln 2)^{1/2}}{c_{ij}} + \frac{2\nu_{ij}v_z(\ln 2)^{1/2}}{c\,c_{ij}}\right)^2\right]}. \tag{15}$$

Observe that

$$\frac{2\nu_{ij}v_z(\ln 2)^{1/2}}{c\,c_{ij}} = v_z\left(\frac{M}{2kT}\right)^{1/2} = y \tag{16}$$

and consequently we obtain the simplification

$$g_{ij}(\nu) = \frac{2}{\pi^{3/2}\,\Delta\nu} \int_{-\infty}^{\infty} \frac{e^{-y^2}\,dy}{1+\left(\frac{x_{ij}+y}{b_{ij}}\right)^2}. \tag{17}$$

The overall stimulated emission cross-section is then given by

$$\sigma = \frac{\lambda^2}{8\pi}\left\{\frac{5}{12}\left(A_{21}g_{21} + A_{22}g_{22} + A_{23}g_{23}\right) + \frac{7}{12}\left(A_{32}g_{32} + A_{33}g_{33} + A_{34}g_{34}\right)\right\} \tag{18}$$

The figures 3,4,5 and 6 are graphs of σ vs frequency change from ν_0 for pressures of 5, 30, 80 and 160 torr and temperature of 293 K.

The equations describing the Voigt profile have been added to the continuous flow laser model laser simulation program. The results have been compared with the standard absorption profile reported in an earlier study. There seems to be no advantage to using the Voigt profile as the laser power output is relatively insensitive to changes in the absorption cross section at the pressures being considered for a space laser. One disadvantage of using the Voigt profile is the excessive numerical computations required by the additional equations.

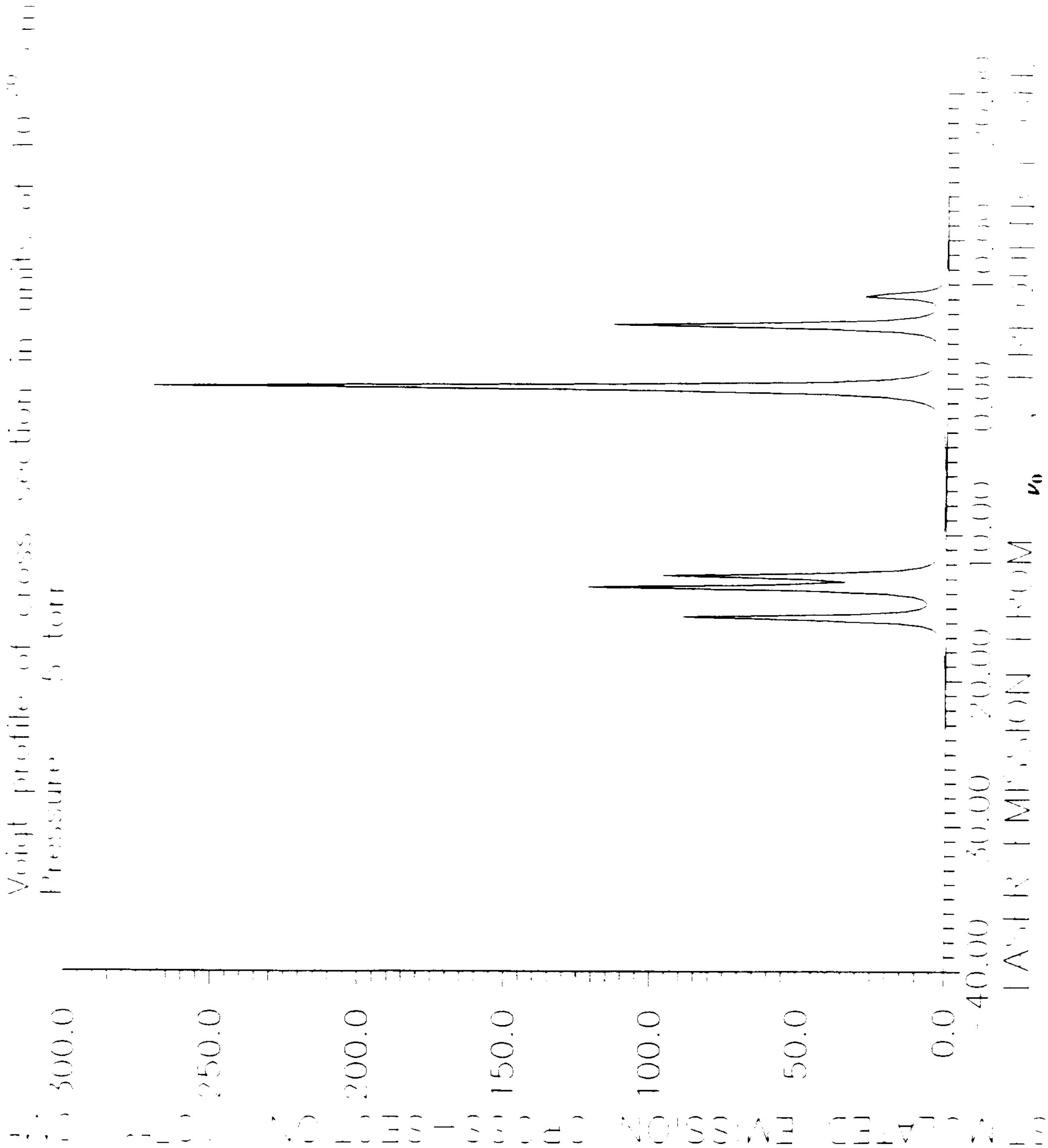

Figure 3 Stimulated emission cross-section $(10)^{-20}$ cm^2 vs laser emission from ν_0, frequency GHz with pressure of 5 torr

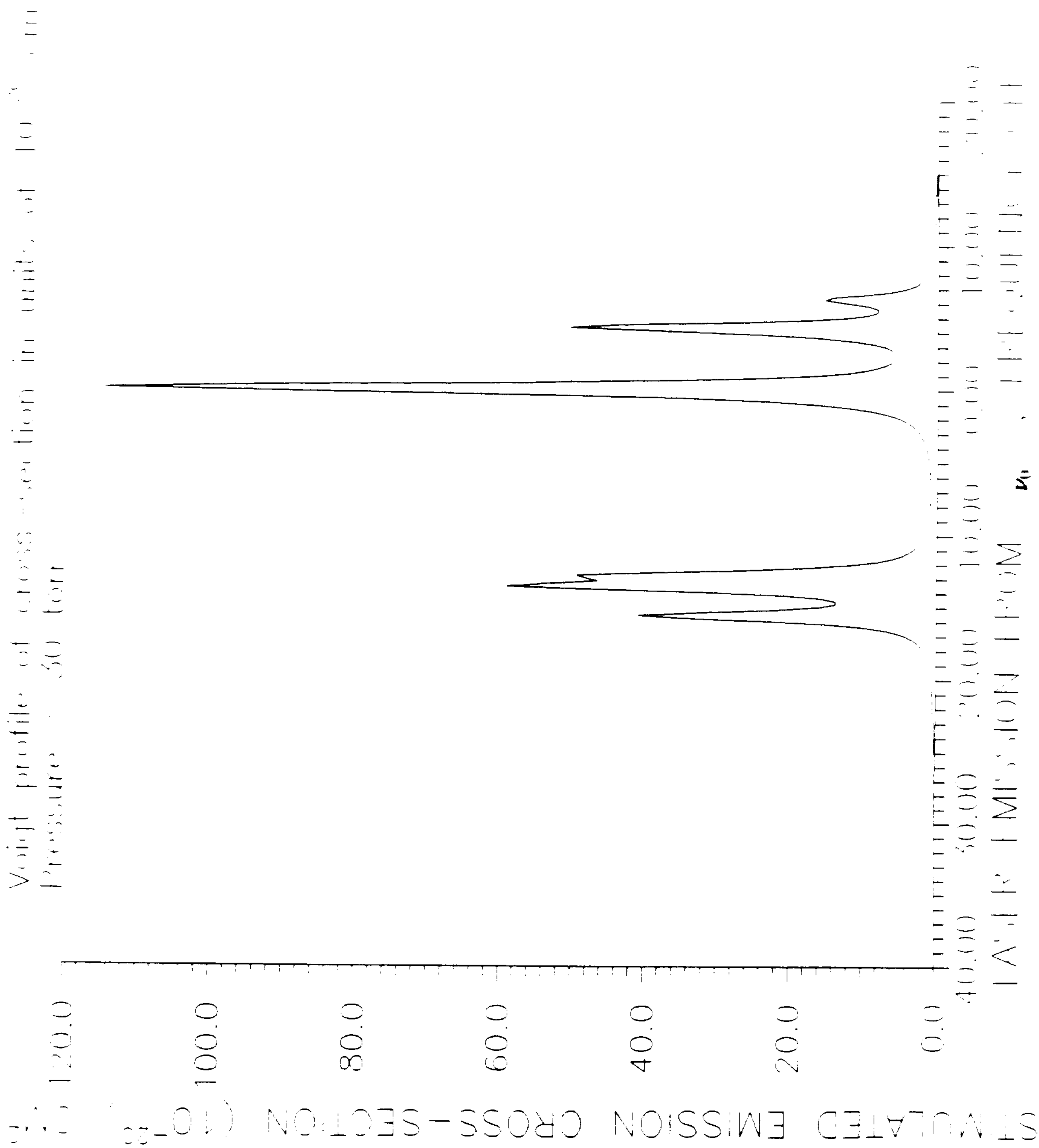

Figure 4 Stimulated emission cross-section $(10)^{-20}\,\mathrm{cm}^2$ vs laser emission from ν_0, frequency GHz with pressure of 30 torr

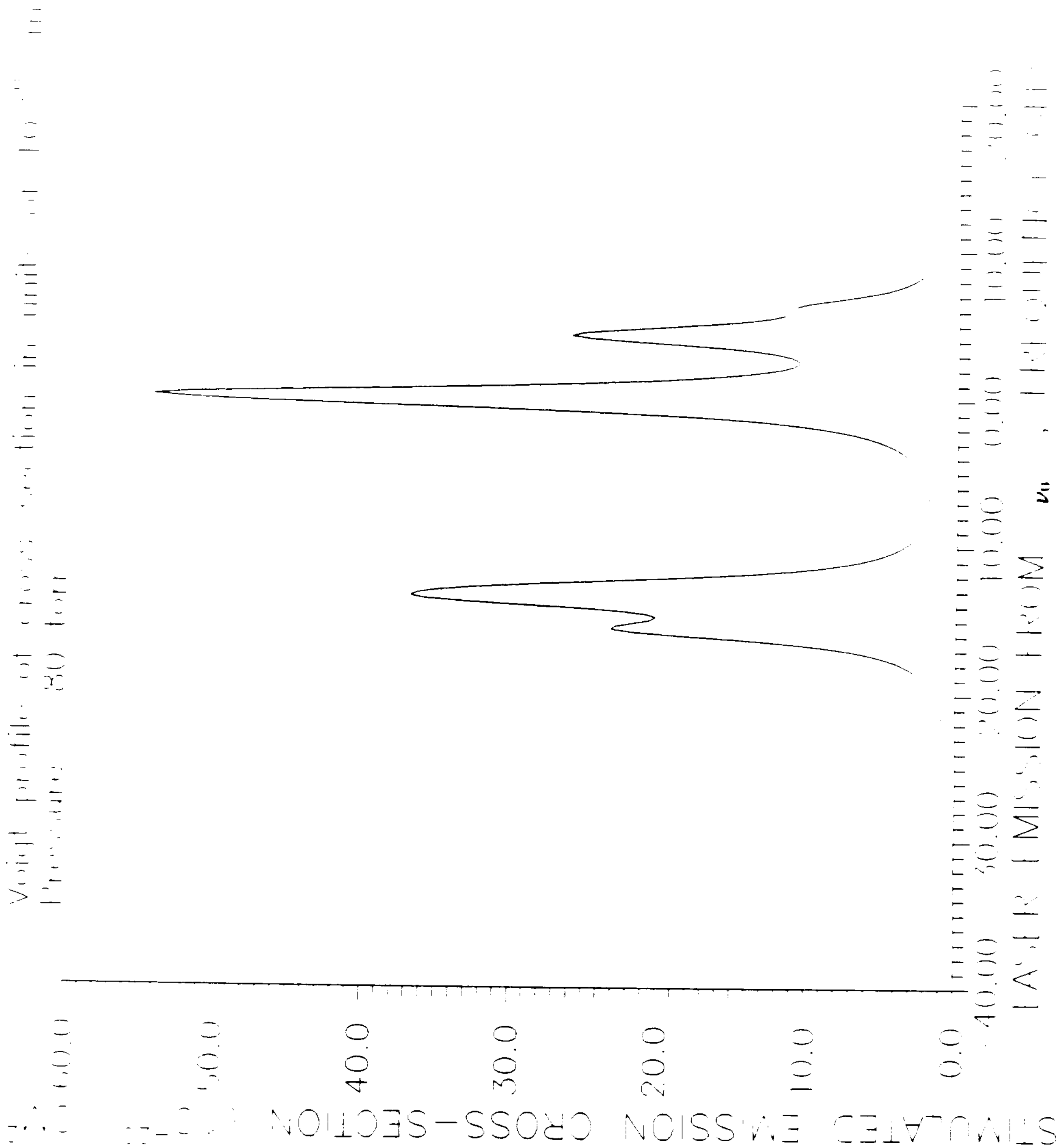

Figure 5 Stimulated emission cross-section $(10)^{-20}\,cm^2$ vs laser emission from ν_0, frequency GHz with pressure of 80 torr

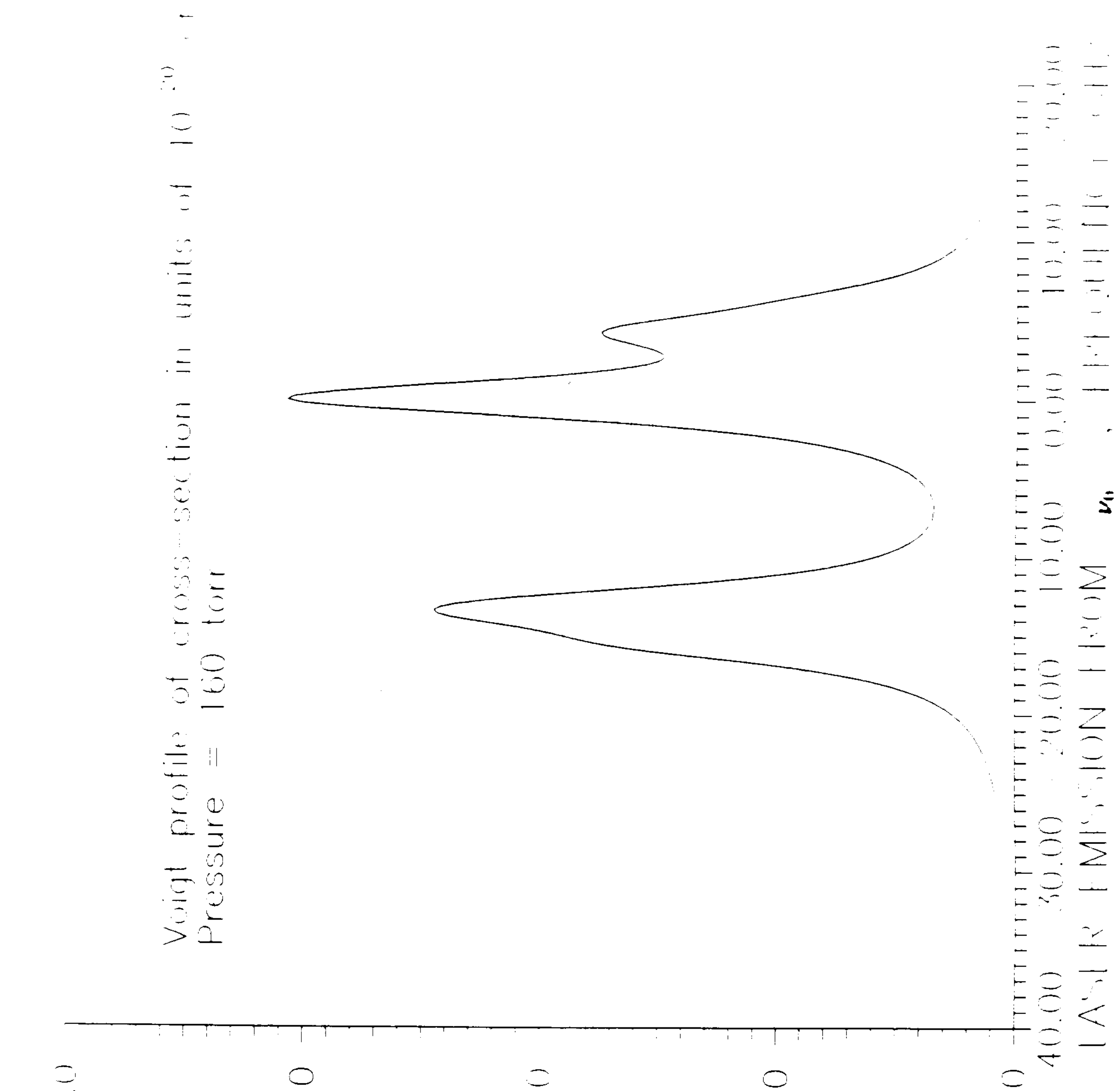

Figure 6 Stimulated emission cross-section $(10)^{-20}\,\mathrm{cm}^2$ vs laser emission from ν_0, frequency GHz with pressure of 160 torr

SIMULATIONS

The current version of the continuous flow laser model computer program was used to compare results from the model with experimental results. The Appendix A contains a fit with the experimental data obtained for the perflouride $i - C_3F_7I$. The Appendix B contains a fit with the experimental data obtained for the perflourides $n - C_3F_7I$ and $n - C_4F_9I$.

The Appendix C contains a simulation, using the laser model, for a $t - C_4F_9$ space laser which is 5 meters in length. The simulation assumes the laser is fully pumped and operating at a pressure of 3.6 torr with a solar concentration of 1370 S.C.

The parameters listed in the Appendics have the following meanings: PTO is the pressure in torr; R2 is reflectivity coefficient of output mirror; OMEG1 is flow velocity upon entering laser; CON is the concentration is solar constants; LC is the length of the laser; ZOL is the half length of the pumped region; T0 is the initial inlet gas temperature; A is the laser radius in cm; $0 \leq XNRHO \leq 1$ is the fraction of incident pump energy left after geometry considerations; FRAC is the fraction of incident radiation energy converted to heat and thermodynamic effects; RAD is the radius along which the numerical integrations were performed; CHI1 is the photo dissociation rate at a given wavelength; CHI2 is the photo dissociation rate at another wavelength; CHI3 is postulated third photo dissociation rate (assumed zero for all fits with experimential data); A00,B00 are coefficients used to calculate the perflouride specific heats at constant volume; KK1 through KK10 are reaction rates; QQ1 through QQ5 are quenching coefficients; and CC1 through CC4 are three body collosion reaction rates.

Bibliography

[1] G. Breederlow, E. Fill, K.J. White, The High-Power Iodine Laser, Springer-Verlag, Berlin, Heidelberg, New York, 1983.

[2] P.W. Milonni, J.A. Eberly, Lasers, John Wiley, 1988.

[3] J.T. Verdeyen, Laser Electronics, Prentice-Hall, 1989.

APPENDIX A: EXPERIMENTAL AND THEORETICAL CURVES FOR i-C_3F_7I

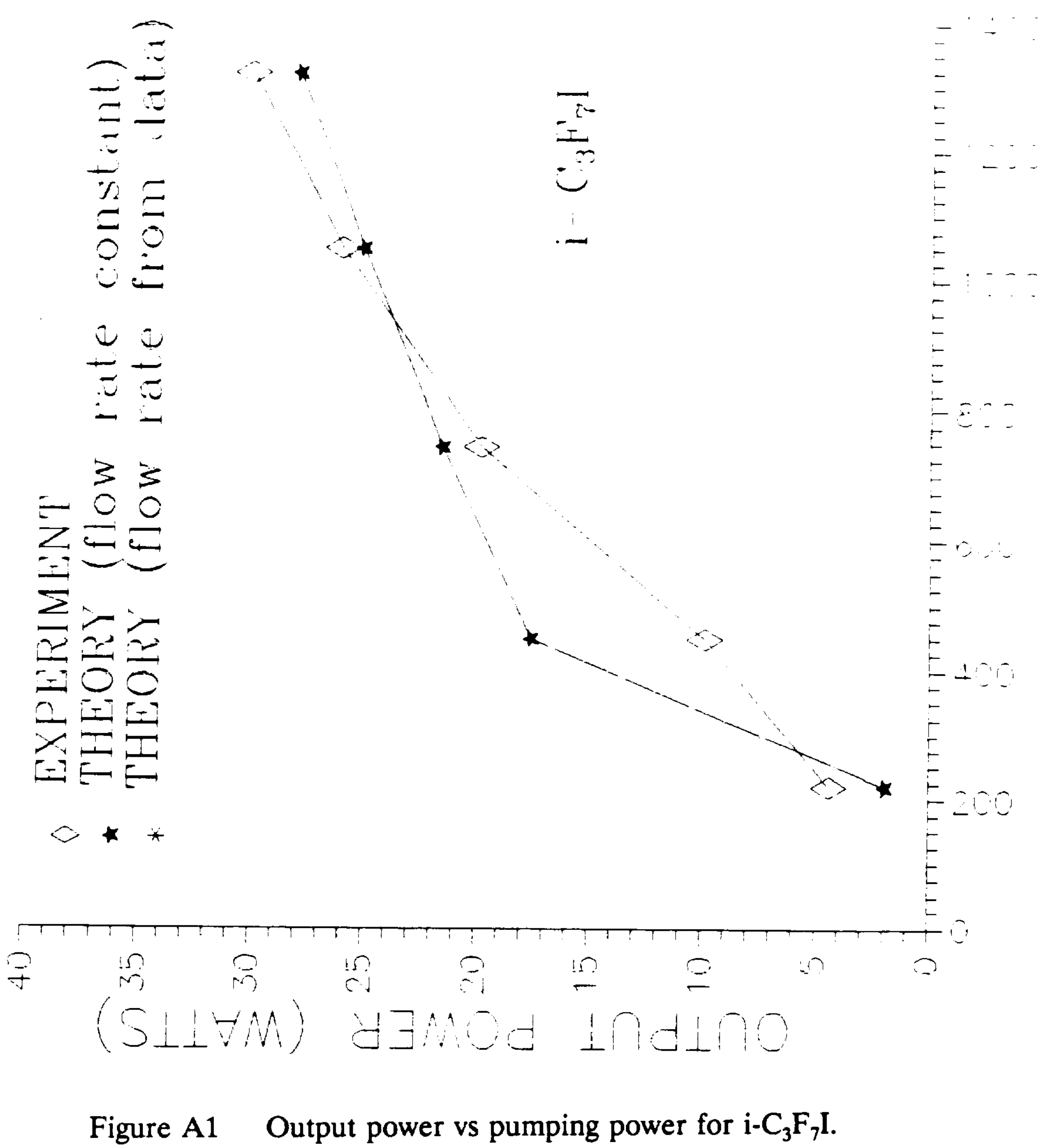

Figure A1 Output power vs pumping power for i-C_3F_7I.

ORIGINAL PAGE IS
OF POOR QUALITY

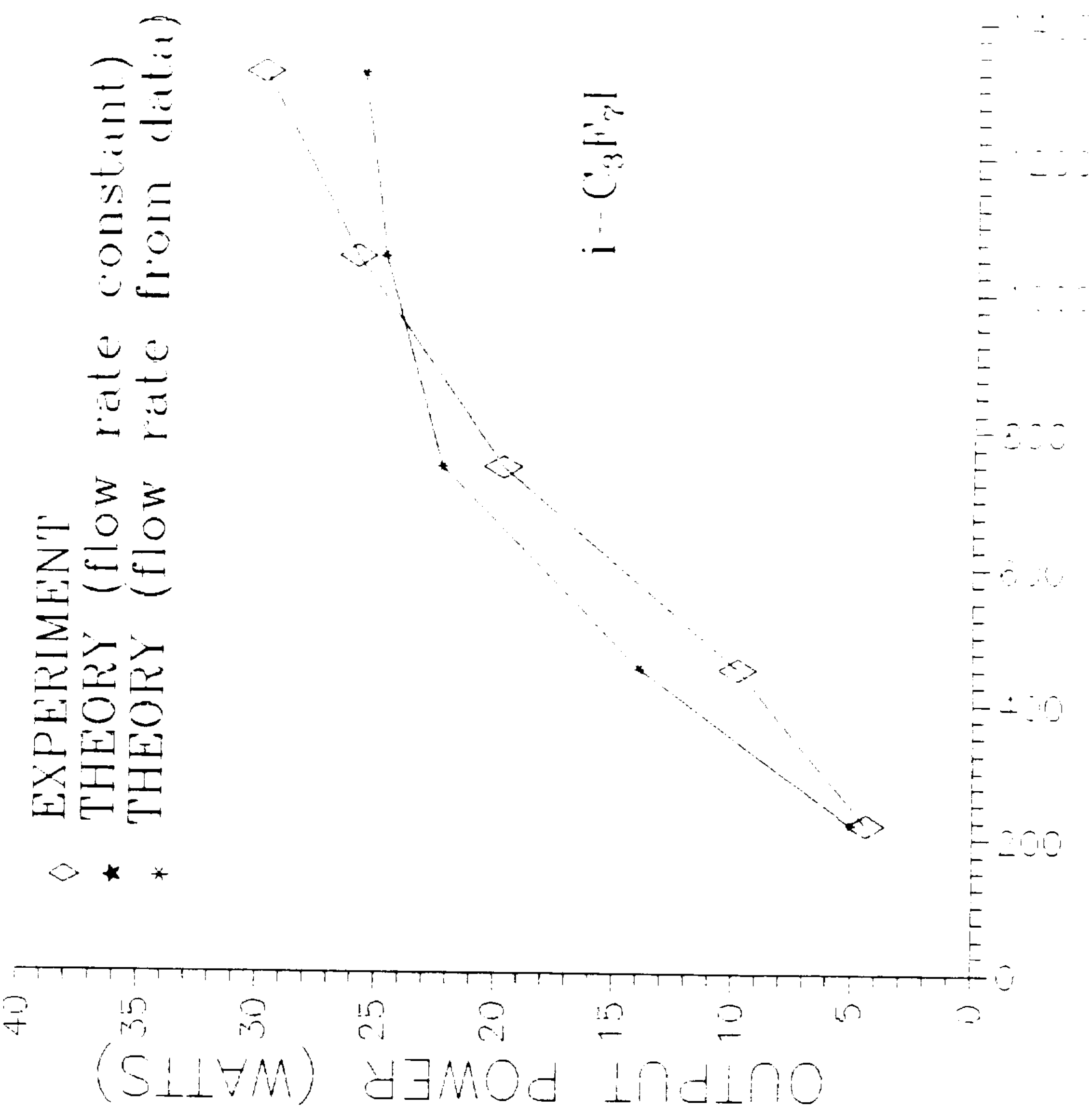

Figure A2 Output power vs pumping power for i-C_3F_7I.

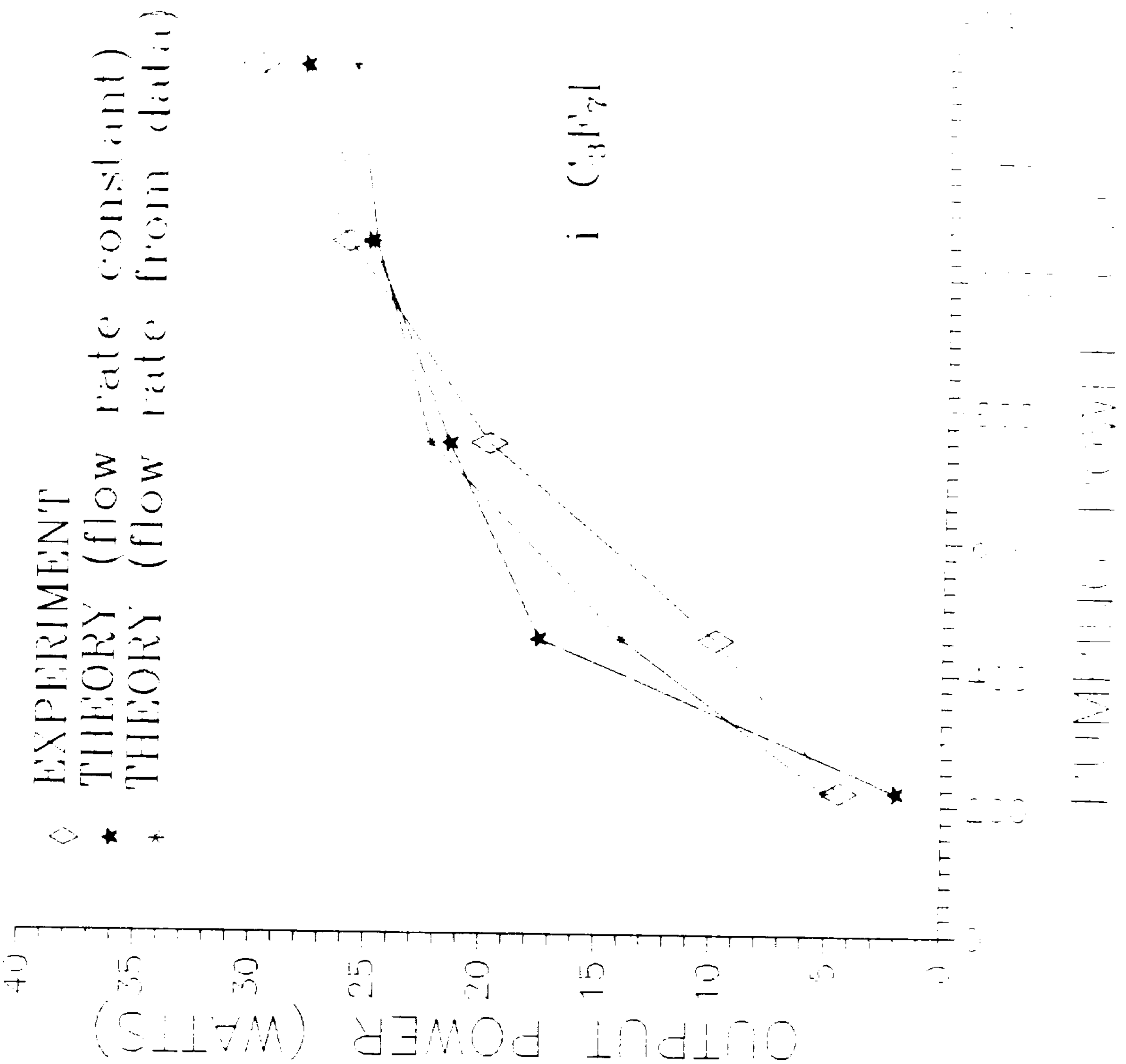

Figure A3 Output power vs pumping power for i-C_3F_7I.

PARAMETERS

PT0 =	3.580000
OMEG1 =	363.200000
C00 =	3.900000E+18
R1 =	1.000000
R2 =	8.500000E-01
TM =	1.500000E-01
XNRHO =	1.000000
CON =	220.000000
LC =	15.000000
ZOL =	7.500000
A =	1.850000
R20 =	0.000000E+00
FRAC =	4.500000E-04
T0 =	300.000000
RAD =	0.000000E+00
V1 =	0.000000E+00
V2 =	0.000000E+00
TTT2 =	1.000000E+18
TTT3 =	1.000000E+18
TTT4 =	1.000000E+18
TTT5 =	1.000000E+18
TTT6 =	1.000000E+18
CHI1 =	1.200000E-02
CHI2 =	1.200000E-01
CHI3 =	0.000000E+00
KK1 =	1.000000E-14
KK2 =	2.300000E-11
KK3 =	6.500000E-13
KK4 =	3.000000E-16
KK5 =	5.000000E-11
KK6 =	0.000000E+00
KK7 =	3.000000E-19
KK8 =	1.600000E-23
KK9 =	1.000000E+15
KK10 =	1.000000E+17
AA0 =	147.230000
BB0 =	1.200000E-03
CC1 =	1.600000E-33
CC2 =	5.700000E-33
CC3 =	0.000000E+00
CC4 =	1.000000
CC5 =	8.000000E-33
QQ1 =	1.700000E-17
QQ2 =	2.890000E-11
QQ3 =	3.700000E-18
QQ4 =	4.700000E-16
QQ5 =	1.600000E-14

Concentration	Experimental Power (Watts)	Calculated Power (Watts)
220	4.42	5.05
450	9.86	14.7
745	19.8	23.65
1050	26	26.02
1320	30	27.2

APPENDIX B: EXPERIMENTAL AND THEORETICAL CURVES FOR n-C_3F_7I and t-C_4F_9I

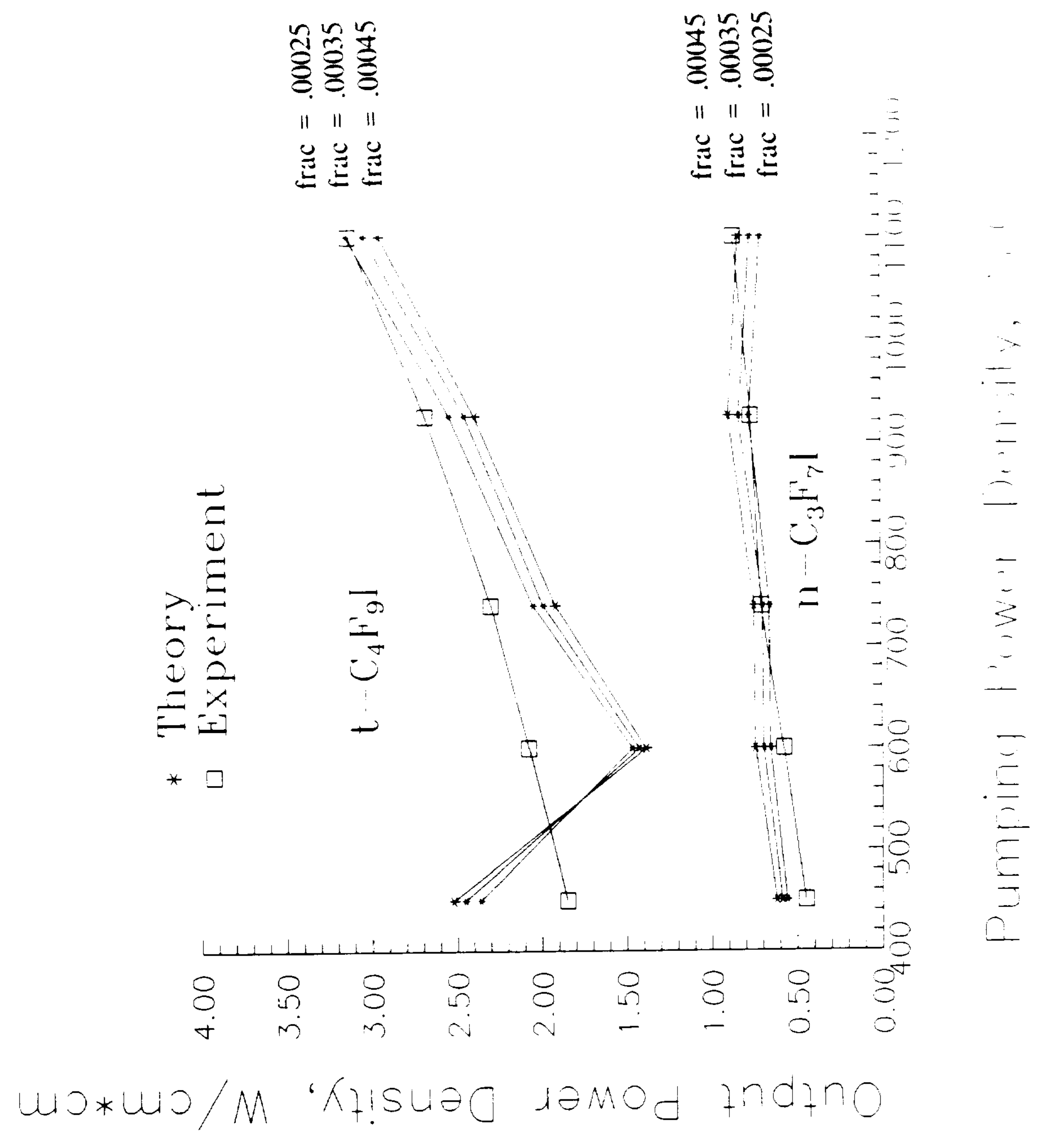

Figure B1 Output power vs pumping power for n-C_3F_7I and t-C_4F_9I.

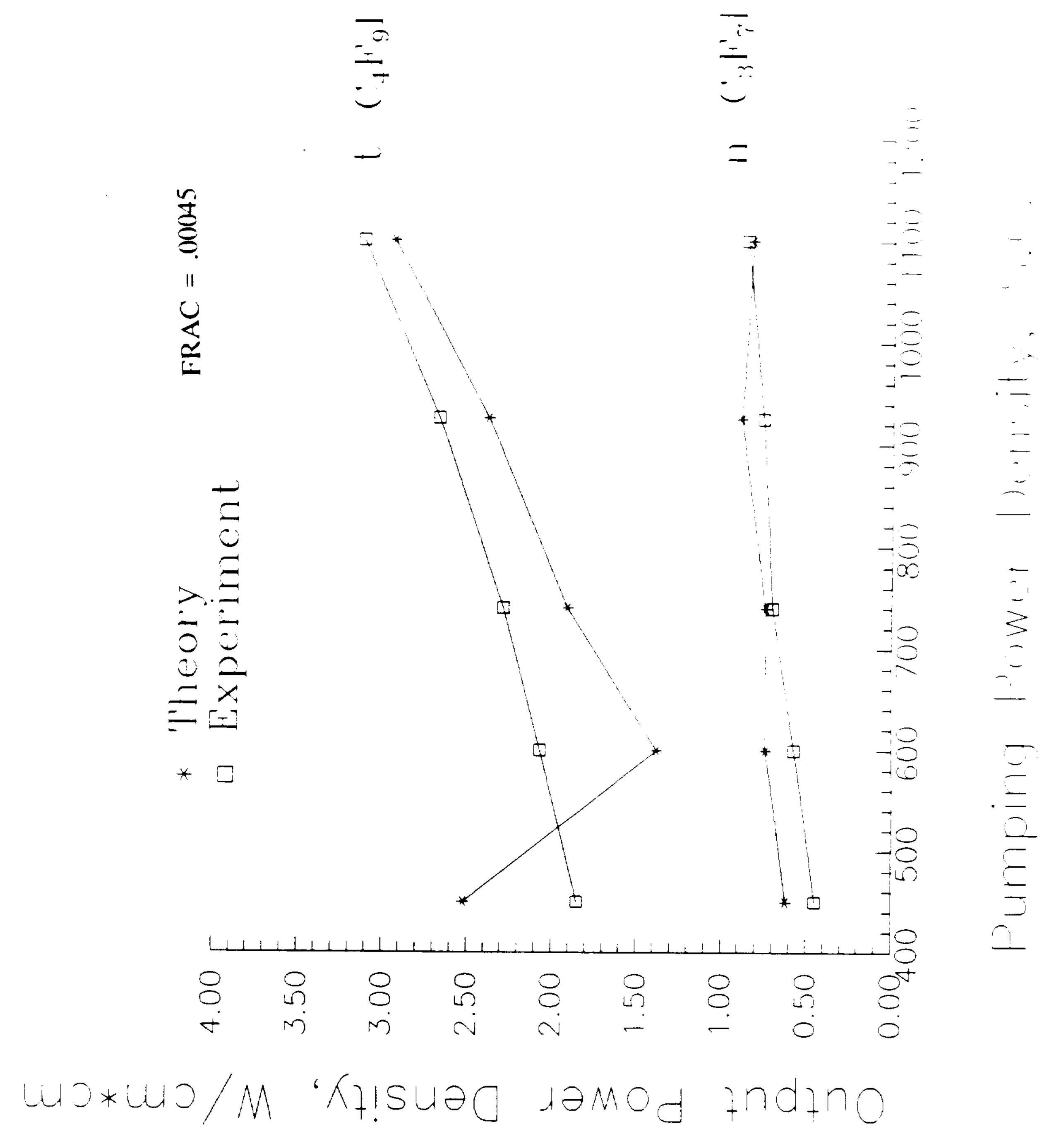

Figure B2 Output power vs pumping power for n-C_3F_7I and t-C_4F_9I.

Parameter	n-C3F7I	t-C4F9I
R1 =	1.000000	1.000000
R2 =	7.000000E-01	7.000000E-01
TM =	3.000000E-01	3.000000E-01
XNRHO =	1.000000	1.000000
LC =	15.000000	15.000000
ZOL =	7.500000	7.500000
A =	1.000000	1.000000
R20 =	0.000000E+00	0.000000E+00
FRAC =	4.500000E-04	4.500000E-04
T0 =	300.000000	300.000000
RAD =	0.000000E+00	0.000000E+00
V1 =	0.000000E+00	0.000000E+00
V2 =	0.000000E+00	0.000000E+00
TTT2 =	1.000000E+18	1.000000E+18
TTT3 =	1.000000E+18	1.000000E+18
TTT4 =	1.000000E+18	1.000000E+18
TTT5 =	1.000000E+18	1.000000E+18
TTT6 =	1.000000E+18	1.000000E+18
CHI1 =	1.200000E-02	1.320000E-02
CHI2 =	1.200000E-01	1.200000E-01
CHI3 =	0.000000E+00	0.000000E+00
KK1 =	1.000000E-14	1.000000E-14
KK2 =	2.300000E-11	6.000000E-12
KK3 =	2.000000E-12	3.000000E-14
KK4 =	3.000000E-16	3.000000E-18
KK5 =	1.000000E-11	1.000000E-11
KK6 =	0.000000E+00	0.000000E+00
KK7 =	3.000000E-19	3.000000E-19
KK8 =	1.600000E-23	1.600000E-23
KK9 =	1.000000E+15	1.000000E+14
KK10 =	1.000000E+17	1.000000E+16
AA0 =	147.230000	183.262400
BB0 =	1.200000E-03	1.398680E-03
CC1 =	1.600000E-33	1.600000E-33
CC2 =	5.700000E-33	5.700000E-33
CC3 =	0.000000E+00	0.000000E+00
CC4 =	1.000000	1.000000
CC5 =	8.000000E-33	8.000000E-33
QQ1 =	1.700000E-17	6.100000E-17
QQ2 =	2.890000E-11	2.890000E-11
QQ3 =	3.700000E-18	3.700000E-18
QQ4 =	4.700000E-16	4.700000E-16
QQ5 =	1.600000E-14	1.600000E-14

	n-C3F7I		
P	CON	OMEG1	POWER DENSITY
5.6	450	663	0.62
5.6	600	663	0.74
6	740	619	0.74
5.8	925	640	0.89
6.4	1100	580	0.83

	t-C4F9I		
P	CON	OMEG1	POWER DENSITY
9	450	550	2.52
4.5	600	733	1.38
4.5	740	733	1.91
4.2	925	707	2.38
4.2	1100	707	2.94

APPENDIX C: SIMULATION OF t-C_4F_9I FIVE METER SPACE LASER, FULLY PUMPED OPERATING AT 3.6 TORR WITH A SOLAR CONCENTRATION OF 1370 SOLAR CONSTANTS

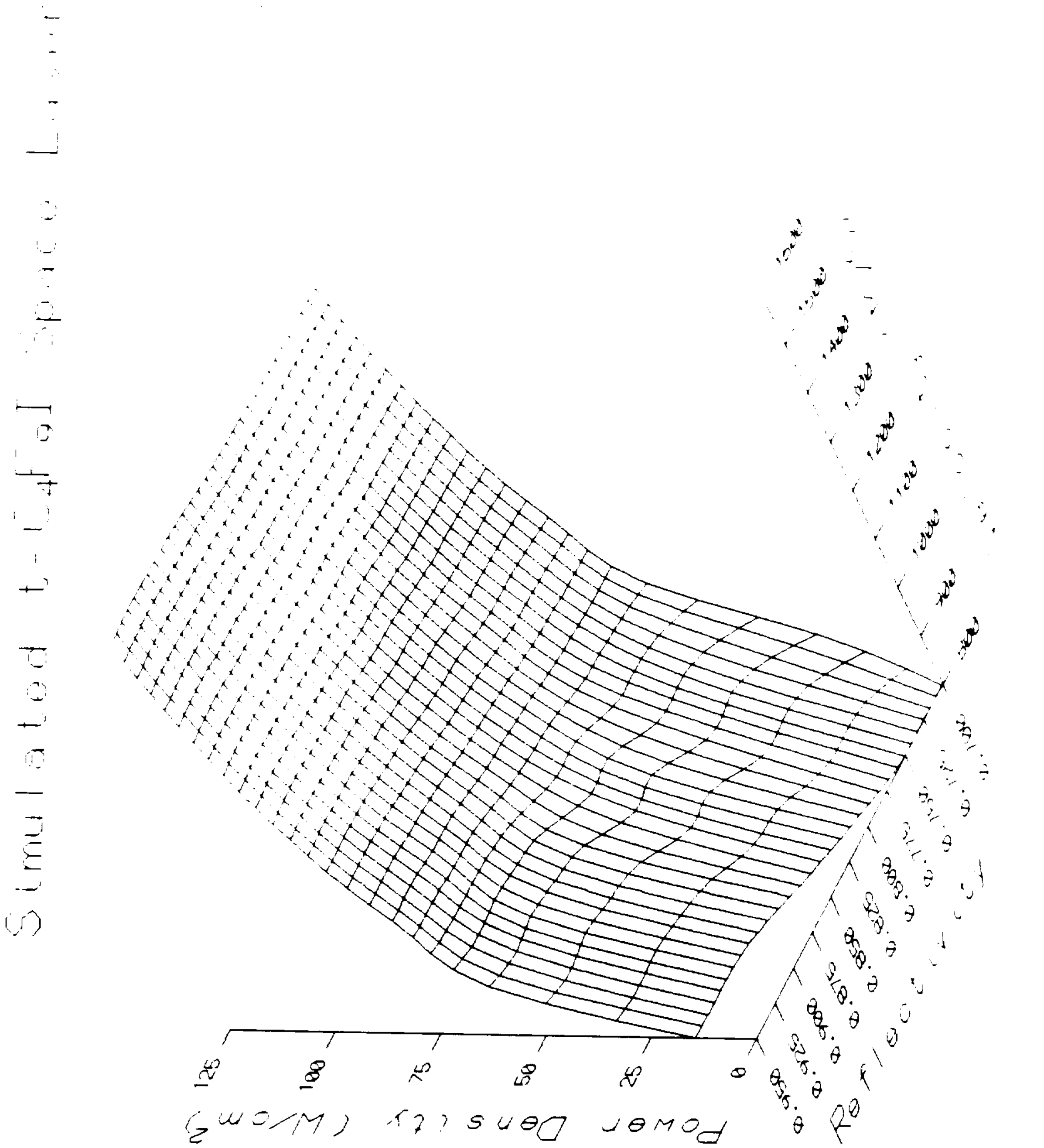

Figure C1 Power density vs velocity and reflectivity for t-C_4F_9I.

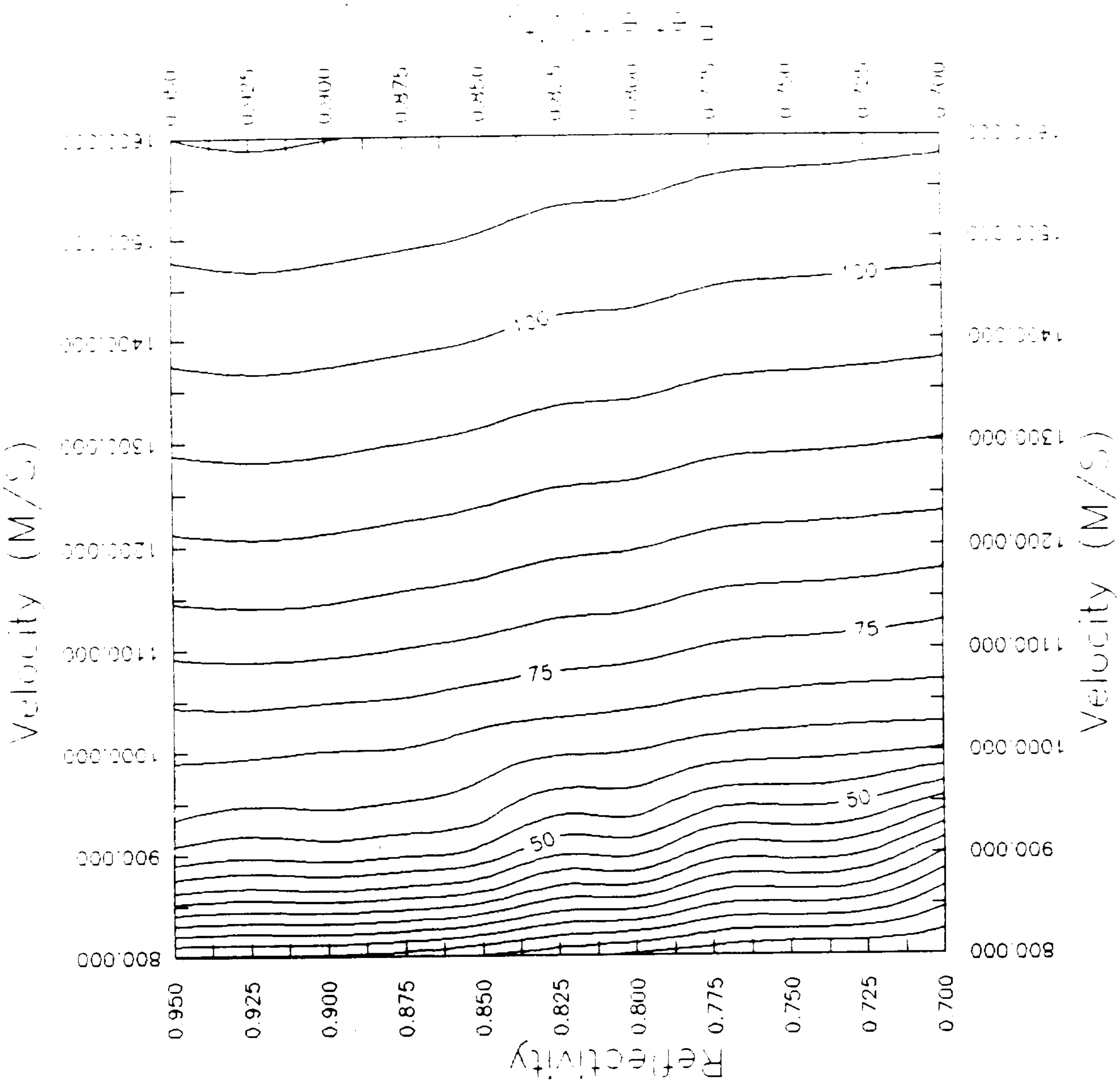

Figure C2 Level curves for power density in Figure C1.

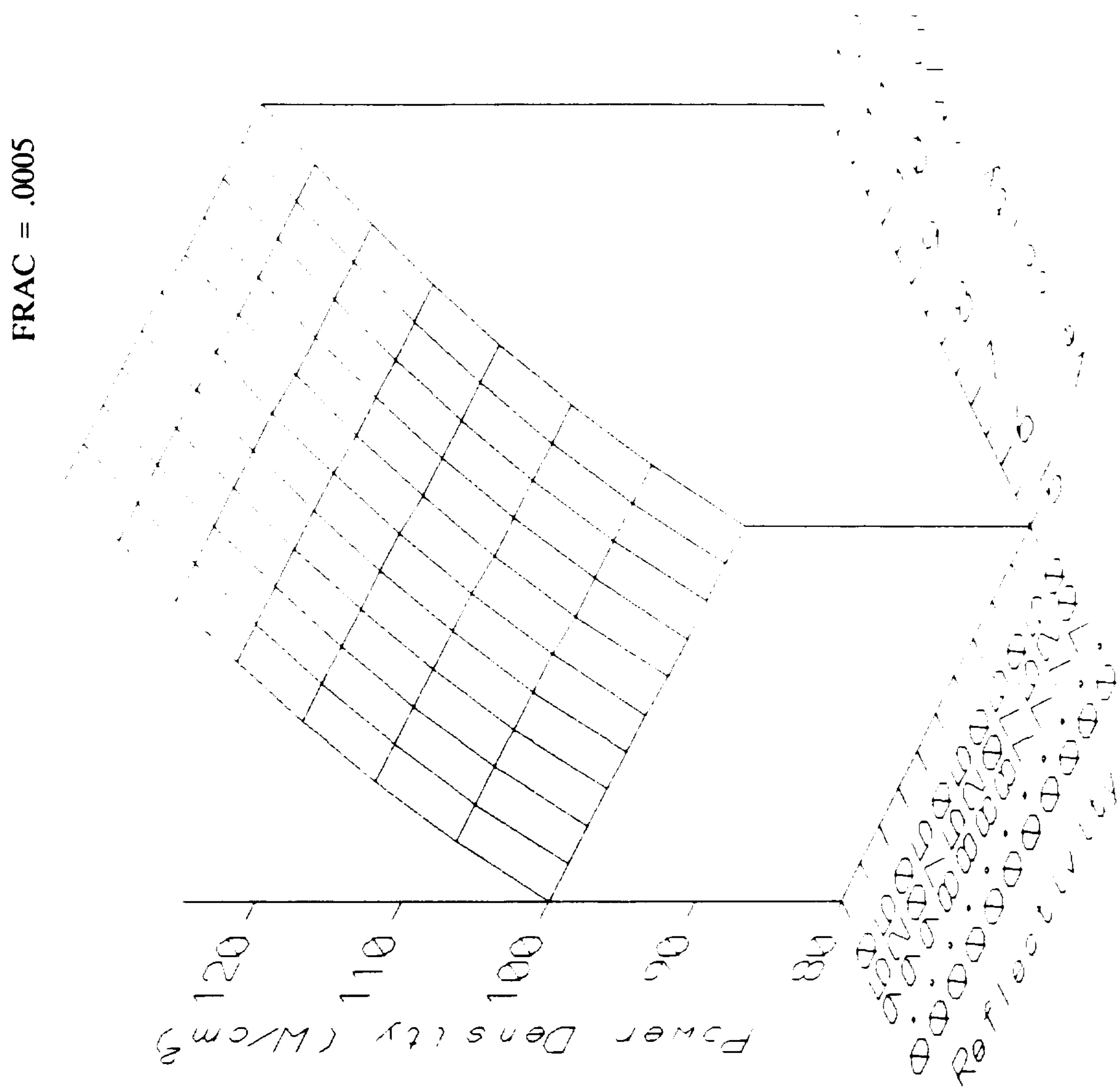

Figure C3 Power density vs velocity and reflectivity for $t\text{-}C_4F_9I$.

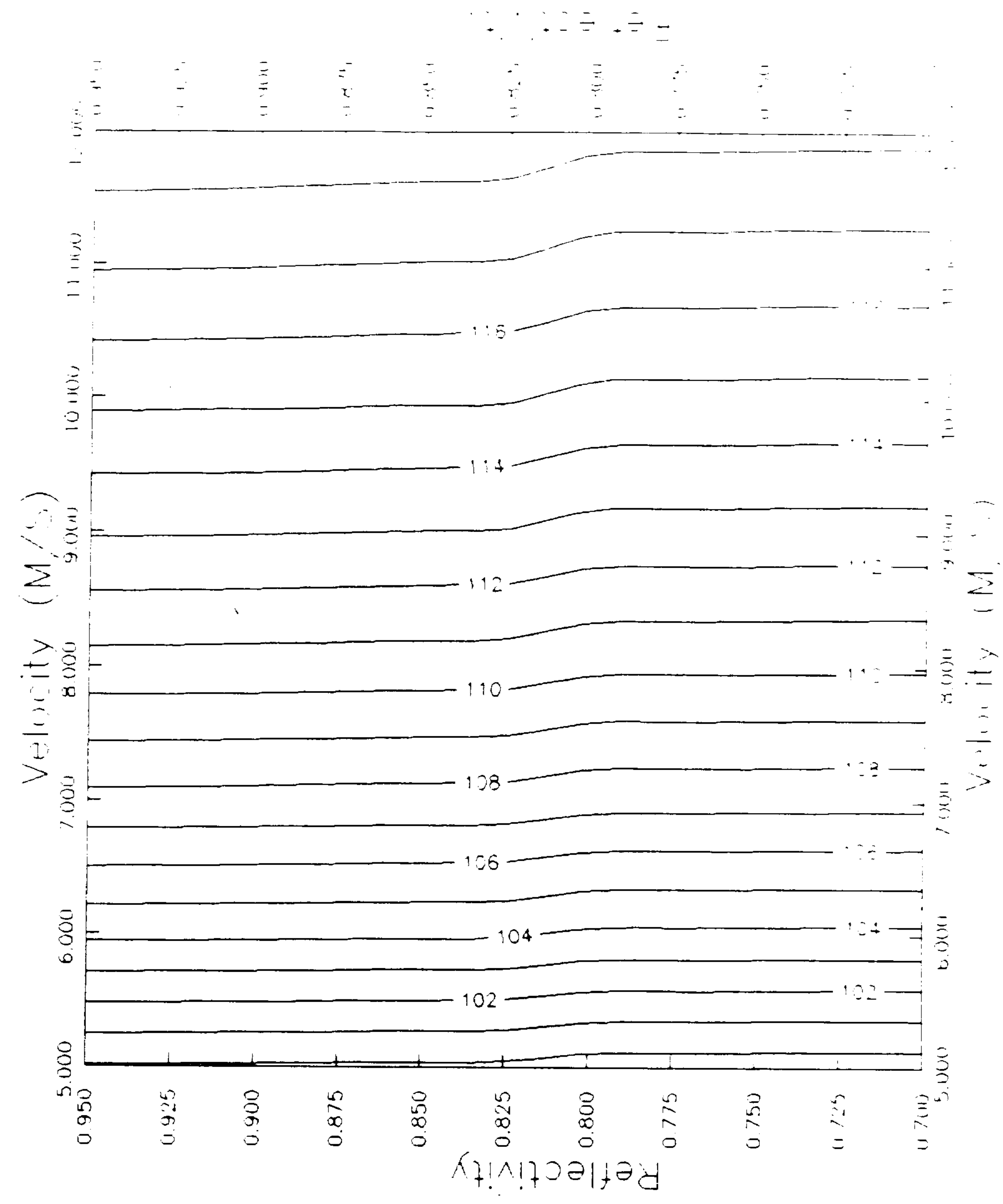

Figure C4 Level curves for power density in Figure C3.

ORIGINAL PAGE IS
OF POOR QUALITY

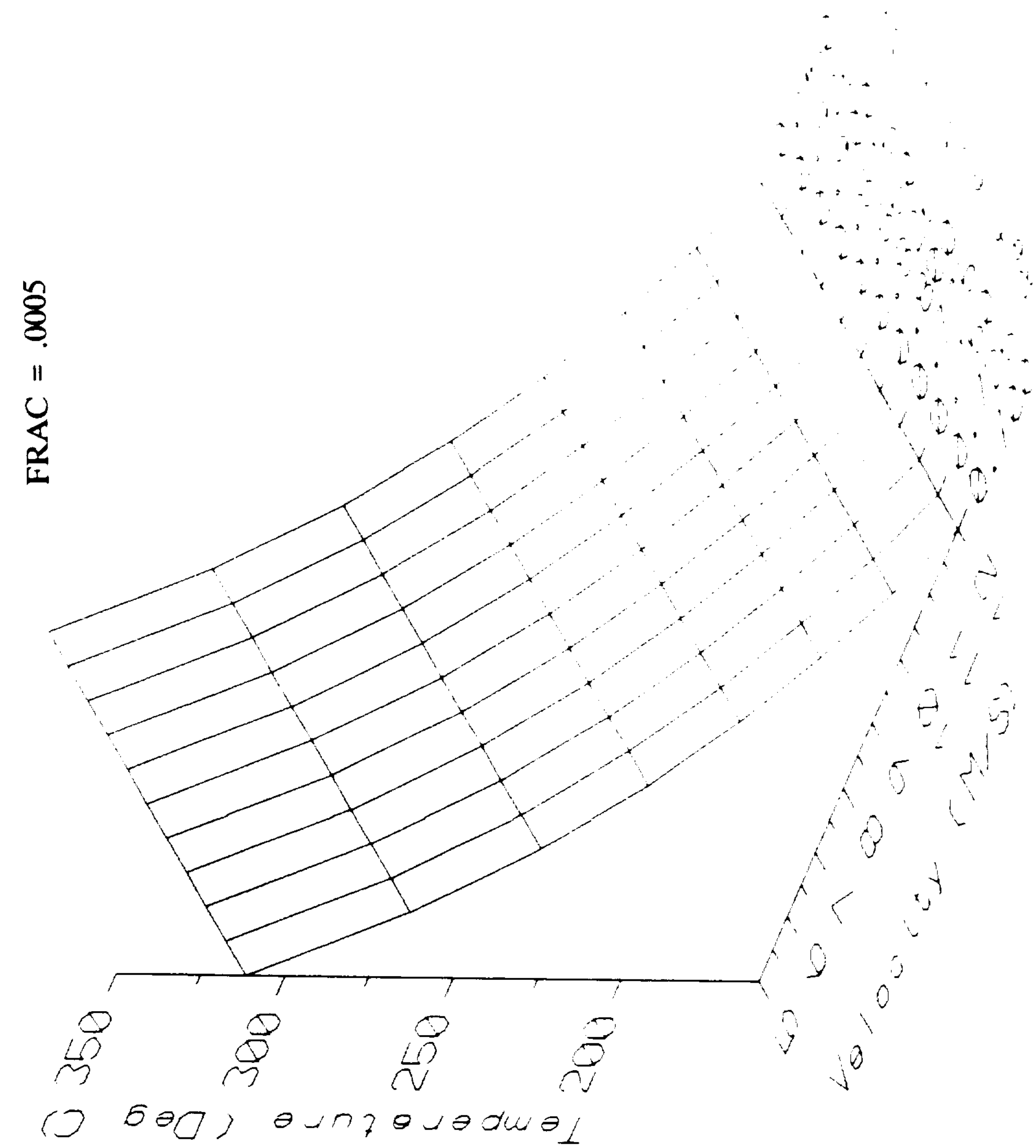

Figure C5 Temperature vs velocity and reflectivity for t-C_4F_9I.

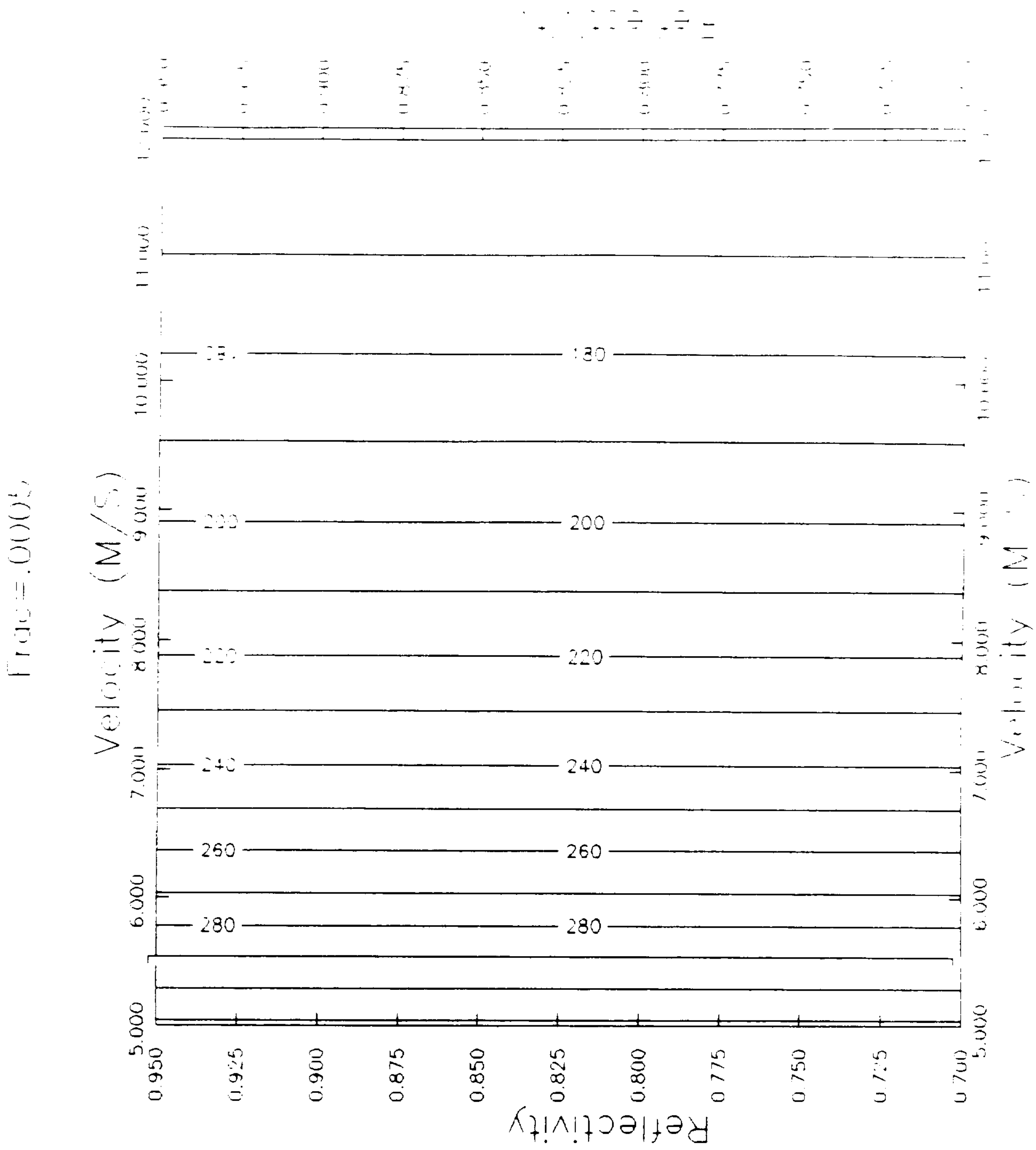

Figure C6 Level curves for temperature in Figure C5.

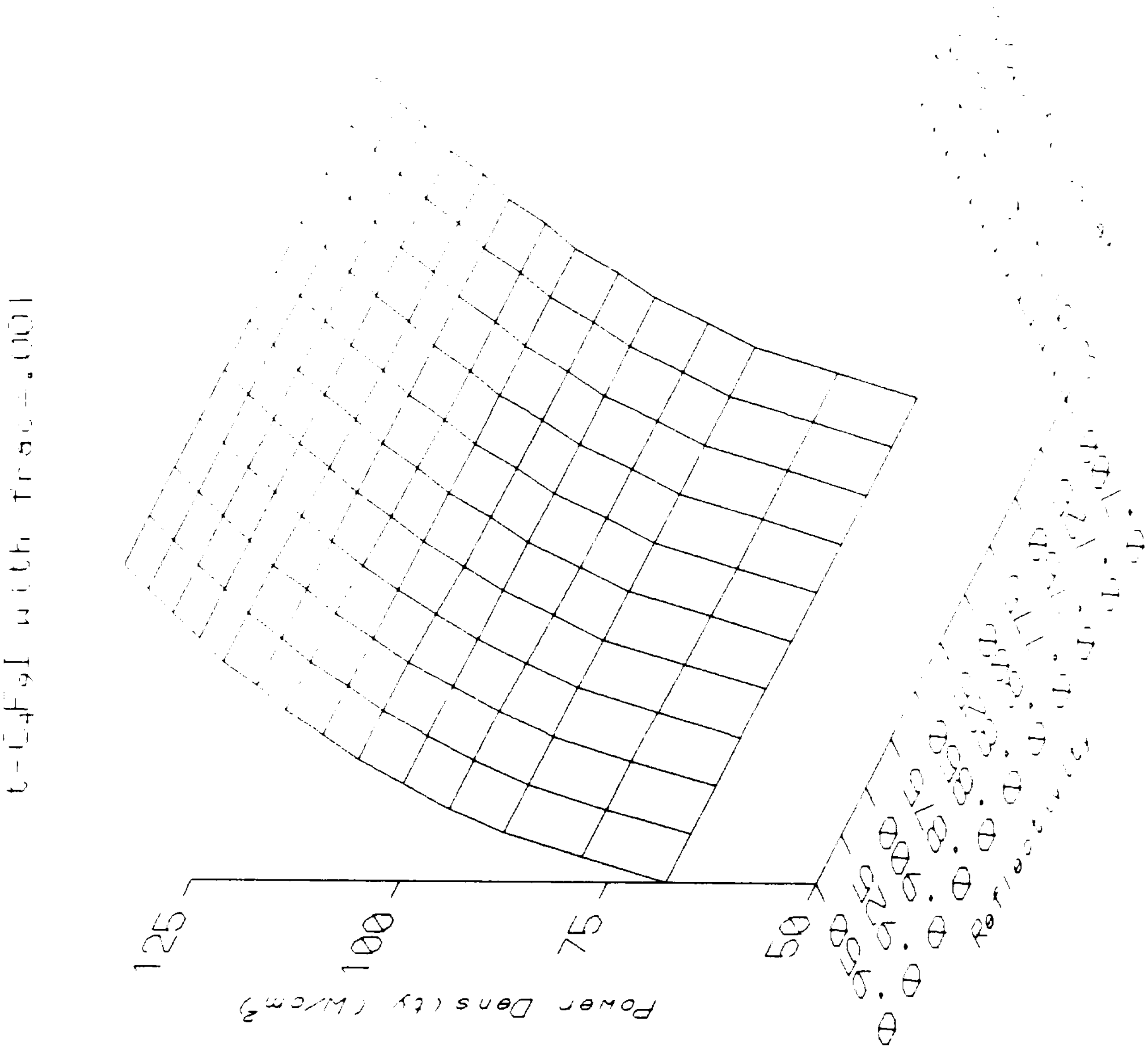

Figure C7 Power density vs velocity and reflectivity for t-C_4F_9I.

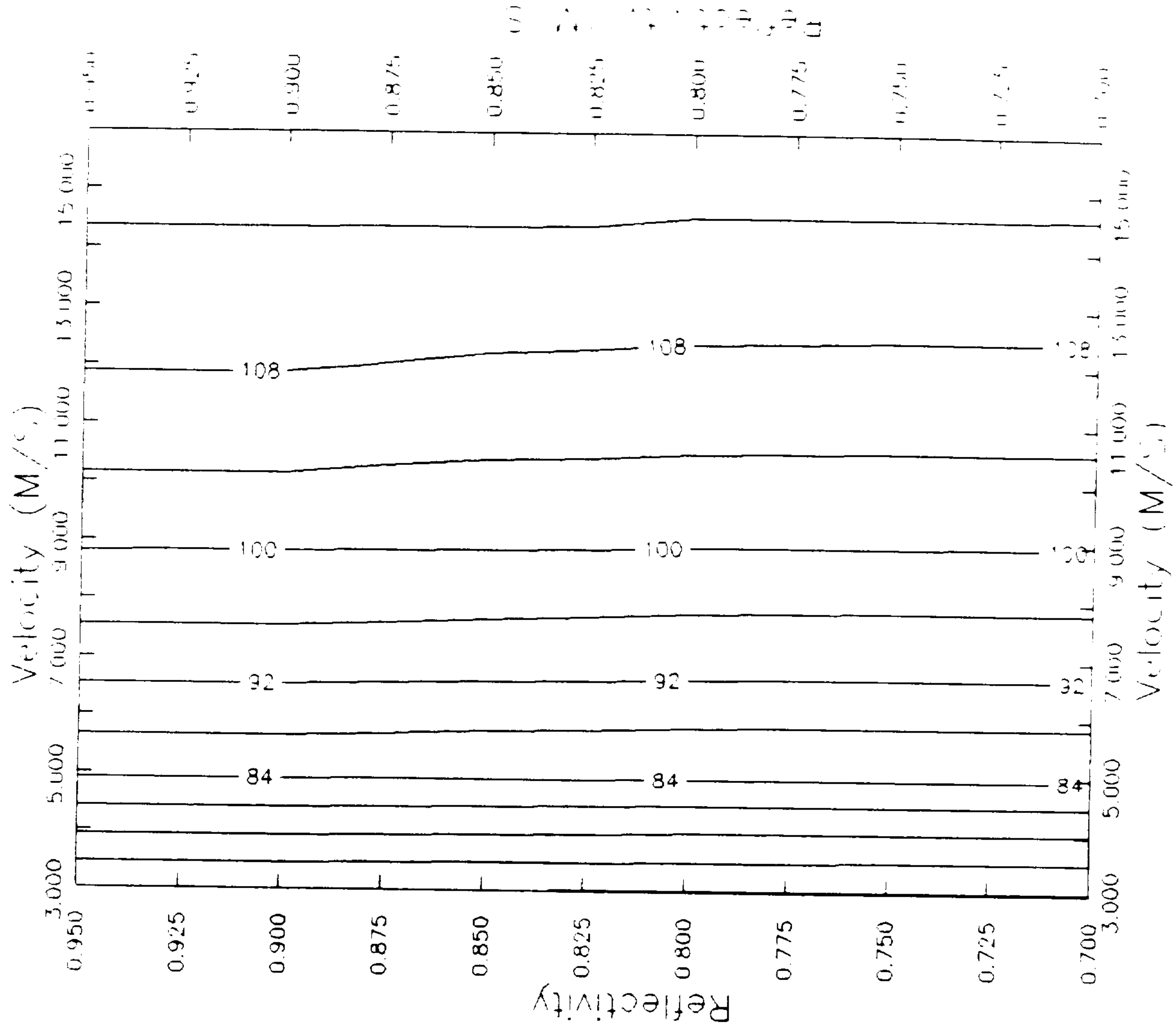

Figure C8 Level curves for power density in Figure C7.

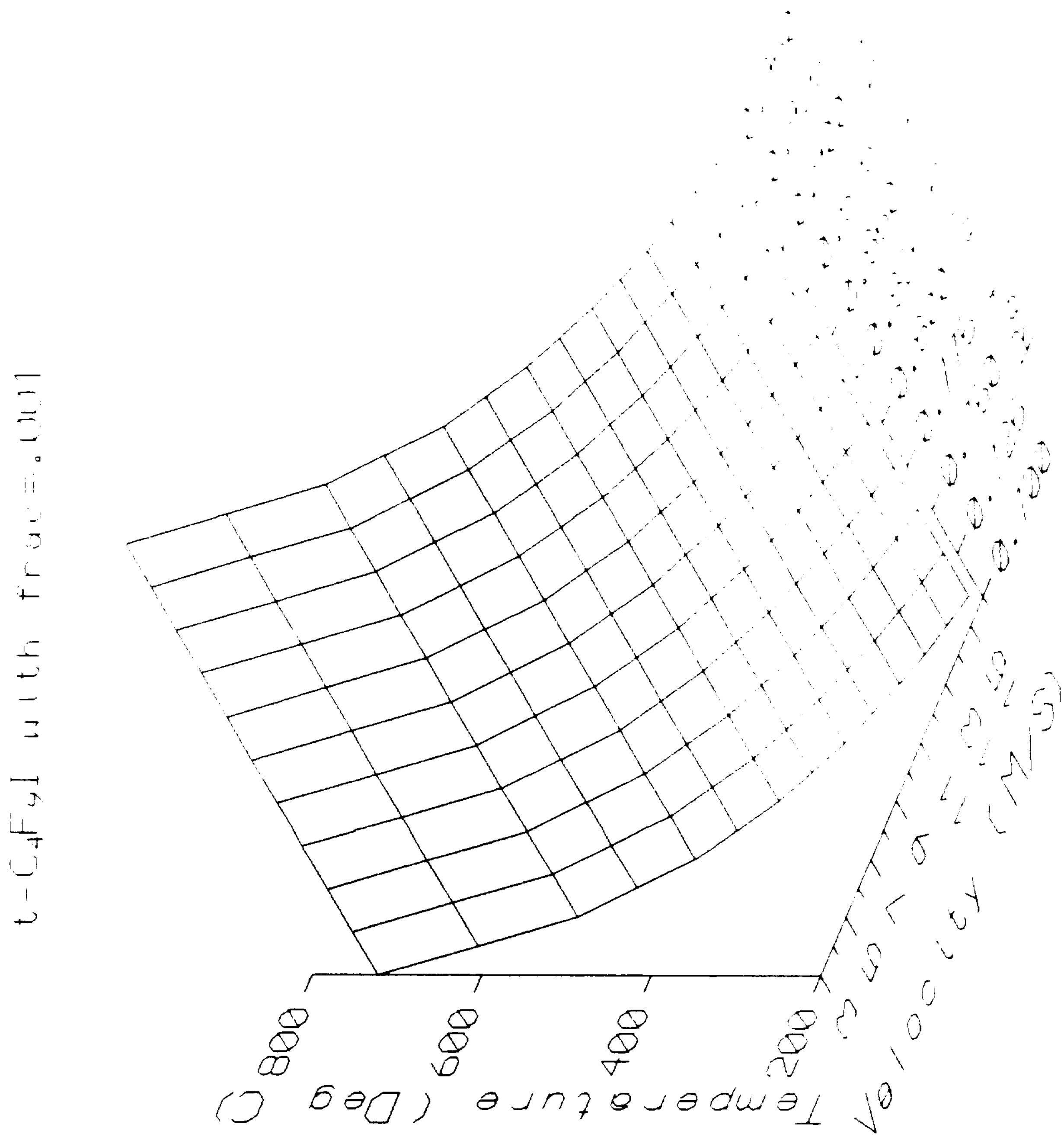

Figure C9 Temperature vs velocity and reflectivity for t-C_4F_9I.

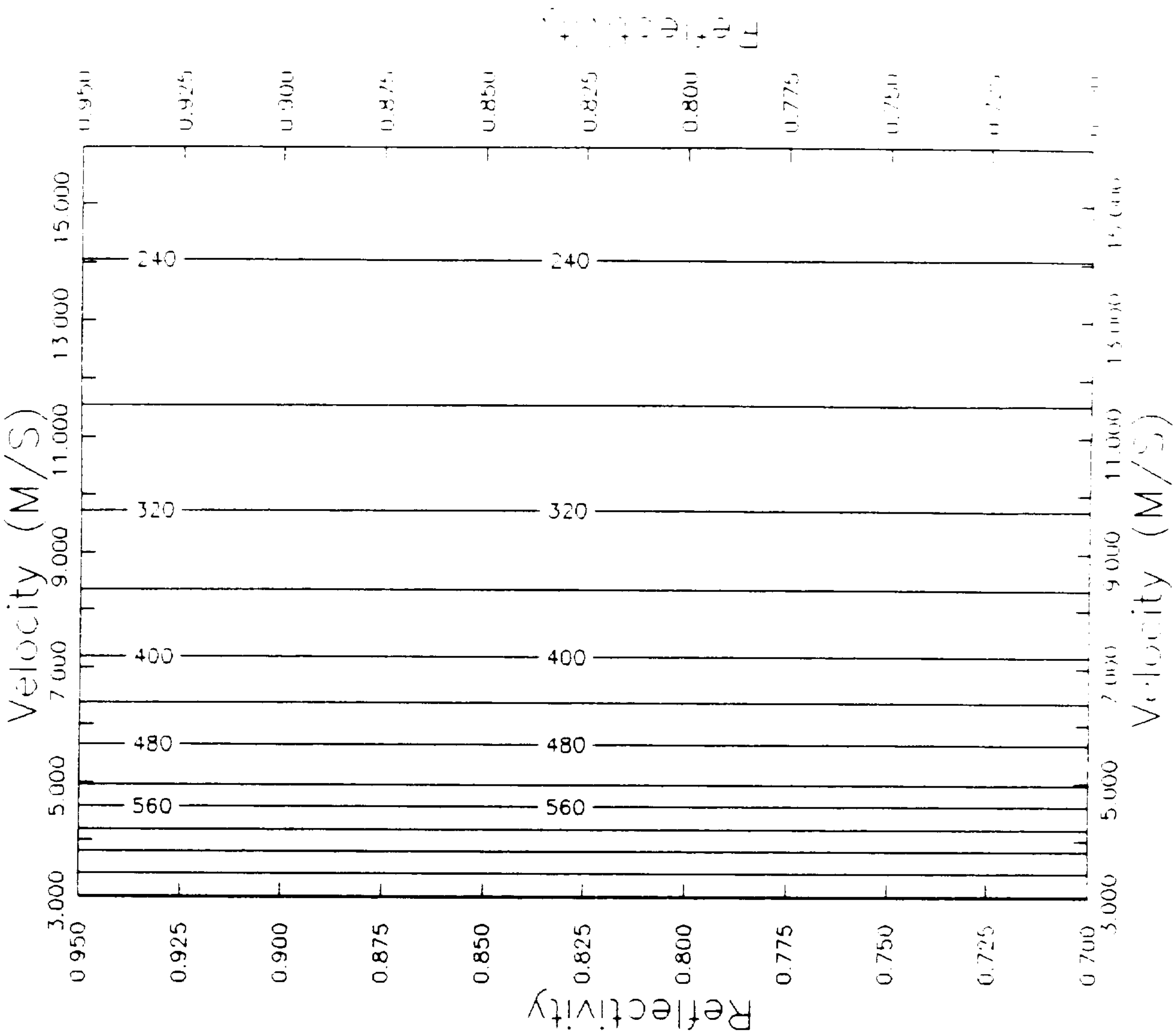

Figure C10 Level curves for temperature in Figure C9.